Eur. Phys. J. D **12**, 425–434 (2000)

THE EUROPEAN PHYSICAL JOURNAL D

EDP Sciences

Binary stopping theory for swift heavy ions

P. Sigmund[1] and A. Schinner[2]

[1] Physics Department, Odense University (SDU), 5230 Odense M, Denmark
[2] Institut für Experimentalphysik, Johannes-Kepler-Universität, 4040 Linz-Auhof, Austria

Received 21 April 2000 and Received in final form 16 June 2000

Abstract. The Bohr theory treats charged-particle stopping as a sequence of interactions with classical target electrons bound harmonically to their equilibrium positions. We demonstrate that equivalent results can be derived on the assumption of free binary collisions governed by a suitable effective potential. This kind of mapping is rigorous in the limits of distant and close collisions and therefore provides a tool to evaluate energy losses *via* binary-scattering theory. This model was developed with the aim of calculating stopping forces for heavy ions at moderately high velocities, where a classical-orbital calculation is typically superior to the Born approximation. The effective potential employed holds equally well for dressed as for stripped ions. Unlike the Bohr theory, the present evaluation avoids a formal division into regimes of close and distant collisions that do not necessarily join smoothly. Moreover, no perturbation expansion is necessary. For these reasons the overall accuracy as well as the range of validity of the Bohr model are significantly enhanced. Extensive tests have been performed, including comparisons with rigorous evaluations of the Z_1^3 effect, with excellent agreement even where such was not necessarily expected. Moreover, credible results have been obtained under conditions where the perturbation expansion shows poor convergence. A comparison with experimental data on O–Al is encouraging, even though shell corrections and projectile excitation/ionization have not yet been incorporated and input has not yet been optimized.

PACS. 34.50.Bw Energy loss and stopping power – 61.85.+p Channeling phenomena (blocking, energy loss, etc.) – 52.40.Mj Particle beam interactions in plasma

1 Introduction

The stopping of swift hydrogen and helium ions in matter is commonly described by the Bethe theory [1] which treats the excitation of target electrons within the first Born approximation. Quantitative agreement can be obtained with numerous experimental results provided that allowance is made for appropriate corrections [2,3]. For ions heavier than helium the range of validity of the Born approximation narrows, the lower limit moving to higher velocities. For the heaviest ions that range reduces practically to zero [4].

On the other hand, it was recognized long ago [5,6] that the criteria for validity of the Born approximation on the one hand, and of a classical-orbital description on the other, are roughly complementary. As a consequence, Bohr's classical theory of particle stopping [7,8] may take over – at least as a feasible starting point – in the velocity range $v < 2Z_1v_0$ where the Bethe theory becomes less accurate. Here, Z_1 is the atomic number of the projectile and v_0 the Bohr velocity.

While recent attempts to estimate stopping forces on the basis of a modified Bohr theory are encouraging [9,10], the Bohr theory in its original form, designed for swift alpha particles, needs significant adjustments in order to allow predictions for heavy-ion stopping. The most obvious corrections all increase in significance with decreasing velocity. Pertinent theoretical efforts have so far focused on screening [9], higher-order perturbation [11], and shell correction [12].

A fundamental aspect of the Bohr theory is the splitting into two regimes for small and large impact parameters: close interactions are taken to follow Rutherford's law,

$$T(p,v) = \frac{2mv^2}{1+(pmv^2/Z_1e^2)^2} \qquad (p \text{ small}) \qquad (1)$$

for the energy loss T *versus* impact parameter p, while distant interactions are described as excitations of harmonic oscillators by a time-varying electric field in the dipole approximation,

$$T(p,v) = \frac{2Z_1^2e^4\omega^2}{mv^4}\left\{\left[K_1\left(\frac{\omega p}{v}\right)\right]^2 + \left[K_0\left(\frac{\omega p}{v}\right)\right]^2\right\}, \qquad (p \text{ large}) \quad (2)$$

where ω is the oscillator frequency and K_0, K_1 are modified Bessel functions in standard notation.

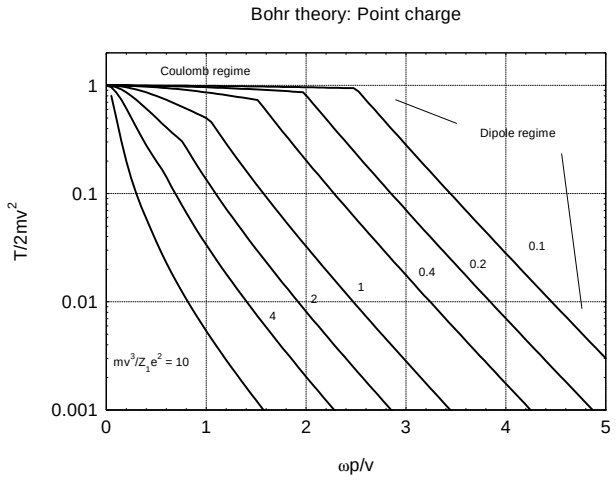

Fig. 1. Energy transfer T per collision event *versus* impact parameter p in Bohr theory with $\xi = mv^3/Z_1e^2\omega = 0.1$ to 10 (right to left).

Figure 1, showing $T(p, v)$ in appropriate dimensionless units, *i.e.* the Bohr parameter $\xi = mv^3/Z_1e^2\omega$ for the beam velocity and $\omega p/v$ for the impact parameter, illustrates the interplay between the two regimes defined by equations (1, 2). It is seen that they join smoothly at high velocities ($mv^3/Z_1e^2\omega \gtrsim 10$) while significant uncertainties must arise in any attempt to interpolate in the velocity range $\xi \lesssim 1$, where a reliable theory is urgently needed and where the Bohr velocity criterion is well fulfilled [8,9].

The existence of the two regimes has been a particularly serious problem in the classical theory of the polarization or Z_1^3 correction (Barkas effect), where the close-collision regime was in fact neglected initially [13,14]. Even though an estimate covering that domain has become available [15], the problem of proper interpolation persists [11]. A similar, although less severe problem has come up recently in connection with the shell correction [12].

Figure 1 indicates that stopping cross-sections

$$S(v) = \int_0^\infty 2\pi p \, \mathrm{d}p \, T(p, v) \tag{3}$$

determined by straight-forward integration under the curves are likely to overestimate the true value within the given physical model, with the expected error increasing with decreasing velocity. Our recent study of the polarization correction [11] suggests an even larger error there, and at the same time the magnitude of the polarization correction was found to become of comparable size with the leading term. This is a strong indicator of the need for an alternative, nonperturbative approach to the Bohr model.

In the present work we report on an attempt to overcome the two problems outlined above by reformulating the Bohr model as a binary-scattering problem governed by an effective potential. We discuss the theoretical basis in some detail and demonstrate that the model rigorously reproduces the predictions of the Bohr theory in the limit of both close and distant interactions. Since our calculation is nonperturbational, higher-order Z_1 effects are implicit. Although the description is not rigorous to higher orders, a stringent test involving existing predictions for Z_1^3 corrections is possible. The model also allows for projectile screening. For both reasons it should qualify for comparison of predicted stopping forces with measurements on heavy-ion beams after proper inclusion of shell corrections and allowance for projectile excitation/ionization.

2 Stripped ions

In qualitative terms the Bohr model characterizes projectile-target interactions by Rutherford's law, truncated at impact parameters beyond the adiabatic radius $a_{\mathrm{ad}} = v/\omega$. One may try to cast this statement into an effective potential of the form [15,16]

$$V_{\mathrm{eff}}(r) = -\frac{Z_1e^2}{r}\mathrm{e}^{-r/a_{\mathrm{ad}}}. \tag{4}$$

It will be shown here that predictions of the Bohr stopping theory may be reproduced quantitatively by characterizing the interaction of the projectile with a target electron as a binary collision governed by the potential equation (4).

Distant interactions may be evaluated by the momentum approximation of classical scattering theory, *i.e.*, first-order perturbation theory which yields a momentum transfer $P_\perp(p, v) = mv\,\theta(p, v)$ normal to the beam direction with a c.m.s. scattering angle[1] θ which is known [17],

$$\theta(p, v) = -\frac{2Z_1e^2}{a_{\mathrm{ad}}mv^2}\, K_1\left(\frac{p}{a_{\mathrm{ad}}}\right). \tag{5}$$

From this follows the energy transfer in the small-angle approximation,

$$T_\perp(p, v) = \frac{1}{2}mv^2[\theta(p, v)]^2 = \frac{2Z_1^2e^4\omega^2}{mv^4}\left[K_1\left(\frac{\omega p}{v}\right)\right]^2, \tag{6}$$

which is identical with the first part of equation (2). We note that also in the Bohr model, that part reflects momentum transfer normal to the beam.

The second term in equation (2),

$$T_{||}(p, v) = \frac{2Z_1^2e^4\omega^2}{mv^4}\left[K_0\left(\frac{\omega p}{v}\right)\right]^2, \tag{7}$$

which reflects momentum transfer $P_{||}(p, v)$ parallel to the beam, does not have a direct analogue in binary scattering. We nevertheless wish to determine its magnitude on the basis of binary-scattering theory. This requires consideration of the physical origin of that term.

Figure 2 shows a sketch of the electron trajectory in the Bohr model following a distant impact. In view of the two

[1] For a heavy projectile the c.m.s. frame coincides with the rest frame of the projectile.

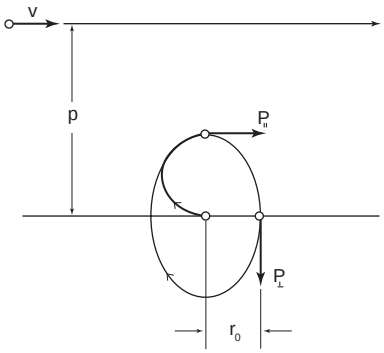

Fig. 2. Elliptic orbit of an excited target electron in the Bohr model.

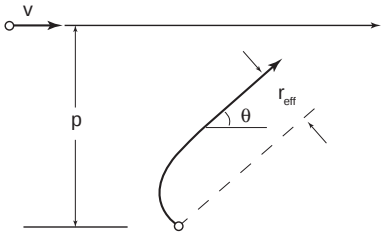

Fig. 3. Orbit of target electron in binary-scattering model.

different Bessel functions entering $P_\perp(p,v)$ and $P_{||}(p,v)$ the asymptotic orbit is elliptical. Since the potential is harmonic, $T_{||}(p,v)$ may alternatively be expressed as the potential energy $(1/2)m\omega^2[r_0(p,v)]^2$ at a distance

$$r_0(p,v) = \frac{2Z_1e^2}{mv^2}K_0\left(\frac{\omega p}{v}\right) \tag{8}$$

from the origin. Note that the electron has received an angular momentum

$$J(p,v) = r_0(p,v)P_\perp(p,v) = -\frac{4Z_1^2e^4\omega}{mv^4}K_0\left(\frac{\omega p}{v}\right)K_1\left(\frac{\omega p}{v}\right). \tag{9}$$

Figure 3 illustrates the same process but now described as a binary-scattering event (without limitation to the small-angle limit). With the momentum transfer $2mv\sin[\theta(p,v)/2]$, the target electron receives angular momentum

$$J(p,v) = 2mr_{\rm eff}(p,v)v\sin\frac{\theta(p,v)}{2}, \tag{10}$$

where the asymptotic impact parameter $r_{\rm eff}(p,v)$ needs to be found by locating the trajectory in the laboratory system. This is a well-established procedure which involves the time integral [18,19]

$$\tau(p,v) = \sqrt{r_m^2-p^2} - \int_{r_m}^{\infty}{\rm d}r \times\left(\frac{1}{\sqrt{1-2V_{\rm eff}(r)/mv^2-p^2/r^2}} - \frac{1}{\sqrt{1-p^2/r^2}}\right), \tag{11}$$

where r_m is the turning point of the trajectory[2], defined as the root of $1-2V_{\rm eff}/mv^2-p^2/r^2=0$. In Appendix A we show that

$$r_{\rm eff}(p,v) = 2\tau(p,v)\cos\frac{\theta(p,v)}{2} - 2p\sin\frac{\theta(p,v)}{2} \tag{12}$$

for all impact parameters. In the small-angle limit this approaches

$$r_{\rm eff}(p,v) \to 2\tau(p,v) - p\theta(p,v). \tag{13}$$

The perturbation expansion of the time integral is sketched in Appendix B. Up to first order in Z_1 for the potential (4), the result is given by

$$\tau(p,v) = \frac{Z_1e^2}{mv^2}\left[K_0\left(\frac{\omega p}{v}\right) - \frac{\omega p}{v}K_1\left(\frac{\omega p}{v}\right)\right]. \tag{14}$$

Insertion of this as well as equation (5) into equation (13) yields

$$r_{\rm eff}(p,v) = \frac{2Z_1e^2}{mv^2}K_0\left(\frac{\omega p}{v}\right) \tag{15}$$

which coincides with $r_0(p,v)$, equation (8).

We thus find that classical small-angle scattering by the screened-Coulomb potential (4) reproduces the predictions of the Bohr model in distant interactions for $T_\perp(p,v)$ as well as the angular-momentum transfer $J(p,v)$. The latter is closely connected to $r_{\rm eff}(p,v)$ which reduces to $r_0(p,v)$ in the small-angle limit. This defines a procedure to specify the potential-energy transfer by adding a term

$$W_0(p,v) = \frac{1}{2}m\omega^2[r_{\rm eff}(p,v)]^2 \tag{16}$$

to the kinetic-energy transfer, which reduces to the Bohr expression for $T_{||}(p,v)$ in the limit of distant interactions.

For closer collisions, both the dipole approximation and the momentum approximation become inaccurate. At the same time, the effects of the oscillator force in the Bohr model and of the screening radius in the binary model become less pronounced, and in the opposite limit of close collisions, both models merge into Rutherford's law.

While the potential-energy transfer vanishes for $p=0$ since $r_{\rm eff}(0,v)=0$ according to equation (12), $r_{\rm eff}$ can become large enough at intermediate impact parameters to cause the potential-energy transfer $W_0(p,v)$ to exceed the ionization energy. This unphysical behavior needs to be removed by restricting the range of validity of the harmonic-oscillator potential. This has been done by means of the *ansatz*

$$\frac{1}{W(p,v)} = \frac{1}{W_0(p,v)} + \frac{1}{U}, \tag{17}$$

where U is the ionization energy.

[2] Equation (11) is formally valid for both attractive and repulsive potentials. For attractive interaction a slight rearrangement can be made to eliminate mutually compensating imaginary terms, *cf.* Appendix B.

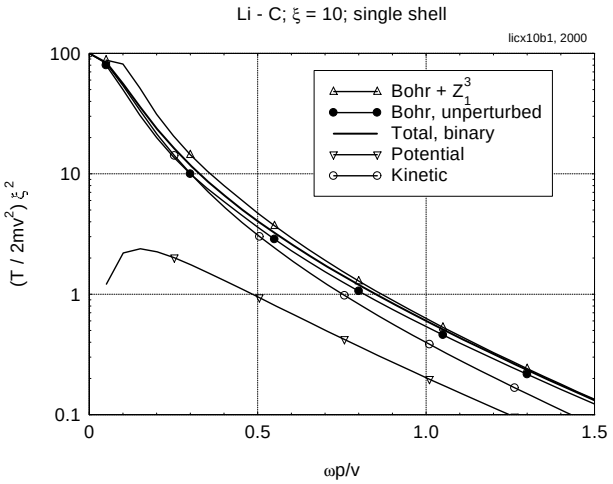

Fig. 4. Energy transfer from bare projectile to target electron *versus* impact parameter in dimensionless units. $\xi = mv^3/Z_1e^2\omega = 10$. See text.

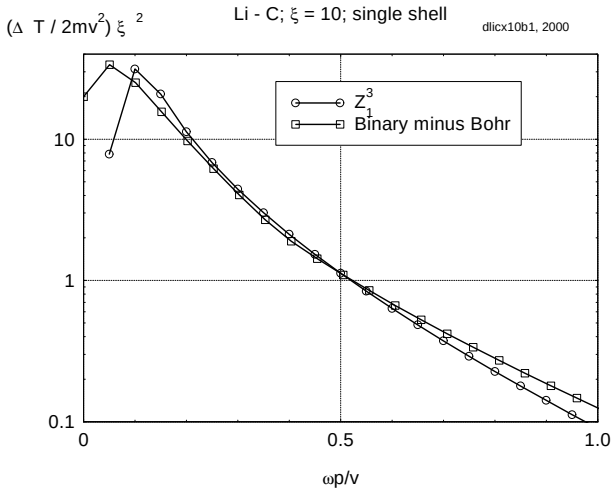

Fig. 5. Difference between total predicted energy transfer and prediction from umodified Bohr model. $\xi = mv^3/Z_1e^2\omega = 10$.

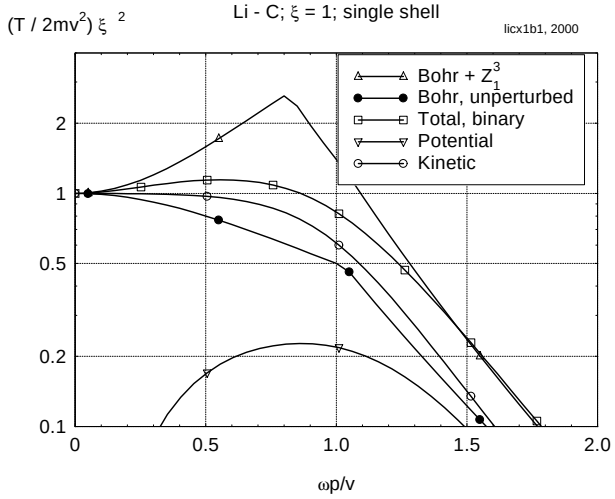

Fig. 6. Same as Figure 4 for $\xi = mv^3/Z_1e^2\omega = 1$.

Determining the energy loss as the sum of a kinetic and a potential contribution,

$$T(p,v) = 2mv^2 \sin^2 \frac{\theta(p,v)}{2} + W(p,v), \qquad (18)$$

with the effective potential equation (4) as a basis, provides a smooth energy-loss function for all impact parameters and velocities, reproducing Bohr's result for distant interactions and approaching free-Coulomb scattering in a physically reasonable way.

While the present procedure evidently circumvents the interpolation problem inherent in the original Bohr model, it is also clear that the scheme – by not invoking a perturbation expansion – must contain higher-order Z_1 contributions. Although there is no reason to expect the same degree of rigor as in the lowest order, the approach appears feasible for not too large corrections. After all, the leading correction term accounts for the collision-induced motion of the target electron *during the interaction time*. This motion is very well approximated in the binary model. Moreover, a successful estimate of the classical Barkas correction to the stopping cross section [15] has been based exclusively on a screened potential of the type of equation (4). Numerical comparisons in the following section will illustrate this point.

3 Calculations

Outside the range of validity of the small-angle approximation, both $\theta(p,v)$ and $\tau(p,v)$ need to be computed numerically. While such a tabulation exists for repulsive interaction [19] we found it necessary to develop a code for accurate numerical integration of the two scattering integrals also for attractive interaction.

Figures 4–6 show calculated energy losses *versus* impact parameter in dimensionless units. Although these computations were nominally performed for Li in C, the only violation of universal scaling is the limitation of the potential-energy transfer *via* equation (17). Therefore the results are quite representative for all ion-target combinations as far as only stripped ions are considered. The target has here been characterized by one resonance frequency. This limits the quantitative significance of these results.

Figure 4 shows results for $\xi = 10$, *i.e.*, a comparatively high projectile speed. It is seen that the energy transfer is predominantly kinetic. The present result, *i.e.*, the solid curve labelled "Total, binary" lies slightly above the Bohr curve, indicating only a small contribution from higher-order perturbations. Also included is a result incorporating the conventional Z_1^3 correction [13], with the close-collision part taken from reference [11] based on a modification of Lindhard's procedure [15]. The latter result lies noticeably above the binary one.

A more detailed view of the same data is shown in Figure 5 where corrections are plotted, *i.e.* the difference between the two predictions underlying Figure 4 and the

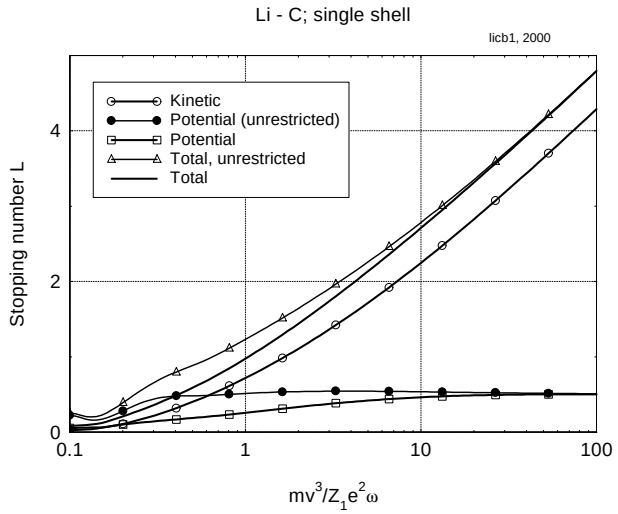

Fig. 7. Stopping number L *versus* ξ for bare ion. See text.

unmodified Bohr theory. With the exception of rather close collisions ($\omega p/v \lesssim 0.1$) the agreement is very good, in particular over the range of impact parameters contributing significantly to the total stopping force. We are confident that the numerical accuracy of both the binary results and the Z_1^3 expansion is good enough to exclude the possibility that the small deviation – which appears to be increasing for $\omega p/v > 0.5$ – reflects computational error[3].

With regard to the behavior at impact parameters $\omega p/v \lesssim 0.1$ we emphasize that the abrupt change in slope in the curve labelled "Binary minus Bohr" is not a feature of the binary model but arises from the subtraction of the Bohr curve. Nonetheless, this hump is much less pronounced than the corresponding one in the curve labelled Z_1^3 evaluated along the scheme presented in reference [11].

Figure 6 shows results corresponding to Figure 4 but now for $\xi = 1$, *i.e.*, a lower velocity. Here, higher-order corrections are significant and may even exceed the lowest-order term in magnitude. The contribution from potential-energy transfer is still of minor significance. The Z_1^3-corrected Bohr curve has now a pronounced cusp as a result of interpolation between poorly overlapping close- and distant-collision regimes. This type of cusp, when noticed recently [11], was in fact our prime motivation to start the present project. The binary model delivers a much more credible interpolation.

Figure 7 shows stopping numbers *versus* ξ, defined *via*

$$L = \frac{mv^2}{4\pi Z_1^2 e^4} \int_0^\infty 2\pi p \, \mathrm{d}p \, T(p, v), \tag{19}$$

calculated with and without the restriction of the potential-energy transfer through equation (17). In the restricted version the potential-energy transfer appears to become significant for $\xi < 1$. It more than doubles in that velocity range when the restriction equation (17) is dropped. Dependent on the velocity range and desired accuracy, refined procedures going beyond equation (17) may eventually be needed.

[3] An independent evaluation of the binary model will emerge in Appendix D.

4 Screened ions

Projectile screening has recently been incorporated into the Bohr theory [9] *via* an interaction potential

$$V(r) = -\frac{q_1 e^2}{r} - \frac{(Z_1 - q_1)e^2}{r} \mathrm{e}^{-r/a_\mathrm{s}}, \tag{20}$$

where $q_1 e$ is the ion charge and a_s a screening radius. Such a potential function was originally proposed in reference [20] to describe the stopping of partially-screened ions in the Born approximation. In the estimates to be reported below we employ a screening radius [9]

$$a_\mathrm{s} = \left(1 - \frac{q_1}{Z_1}\right) a_\mathrm{TF}, \tag{21}$$

where $a_\mathrm{TF} = 0.8853 a_0 / Z_1^{1/3}$ is the Thomas-Fermi radius of a neutral projectile atom. This screening radius differs from the one employed in reference [20].

An effective potential accounting for harmonic binding as well as screening is given by

$$V_\mathrm{eff}(r) = -\frac{q_1 e^2}{r} \mathrm{e}^{-r/a_\mathrm{ad}} - \frac{(Z_1 - q_1)e^2}{r} e^{-r/a} \tag{22}$$

with

$$\frac{1}{a^2} = \frac{1}{a_\mathrm{ad}^2} + \frac{1}{a_\mathrm{s}^2} \cdot \tag{23}$$

Intuitive arguments in favor of this *ansatz* were put forward previously [11]. It is demonstrated in Appendix C that the equivalence of the Bohr theory and a binary-collision model, based on unscreened Coulomb interaction and the potential (4), respectively, remains valid to the same degree of rigor for screened interaction, based on the potentials (20) and (22, 23).

Figure 8 shows a comparison between the calculated energy transfer for a neutral projectile with that of the corresponding stripped ion discussed in Figure 4. Results from the present model are compared with the Z_1^3-corrected Bohr theory [11]. It is seen that the excellent agreement between the binary curve and the Z_1^3 approximation holds down to significantly smaller impact parameters for the neutral projectile than for the stripped ion. This is caused by a weaker potential due to screening (*cf.* also Appendix D).

Figure 9 shows calculated stopping numbers for fully stripped and neutral ions ("frozen charge states") as well as for ions carrying the mean equilibrium charge, the latter being approximated by a Bohr-type relation,

$$\langle q_1 \rangle = Z_1 \left(1 - \mathrm{e}^{-v/Z_1^{2/3} v_0}\right), \tag{24}$$

which has proven useful in our earlier work [10,11]. It is seen again that the Z_1^3 estimates lie significantly above the binary results in all cases.

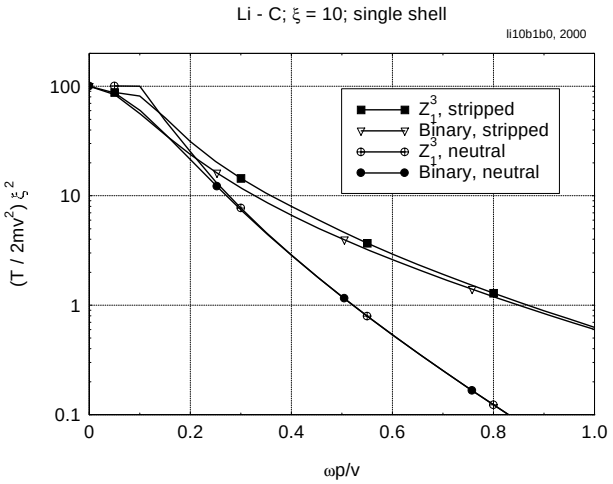

Fig. 8. Energy transfer for neutral compared with stripped projectile. Notation as in Figure 4.

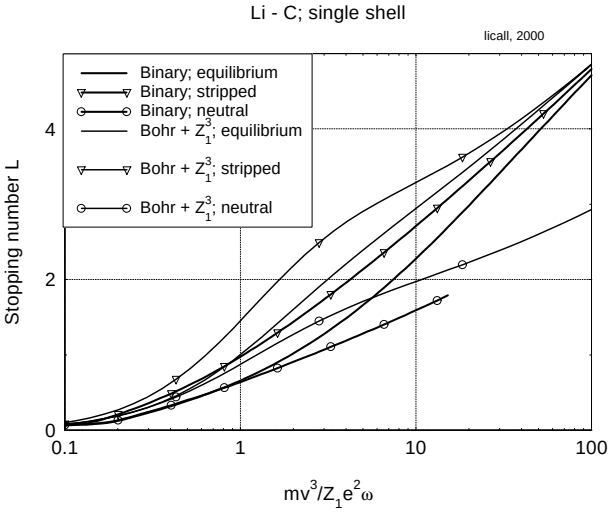

Fig. 9. Stopping number *versus* ξ for frozen charge states $q_1 = Z_1$ (stripped) and $q_1 = 0$ (neutral) as well as for equilibrium charge equation (24).

5 Discussion

While a detailed comparison with experiments requires a number of corrections that are outside the scope of the present paper [10] we shall at least try to indicate to what extent the binary model has a chance to improve agreement with experiment. Figure 10 shows experimental stopping forces for oxygen ions in aluminium tabulated in reference [21,26] and three theoretical curves with comparable numerical input. Pertinent target data employed are listed in Table 1. All curves refer to ions in the mean equilibrium charge state defined by equation (24).

The curve labelled "Bohr", which here incorporates screening and shell summation but no polarization effect, seemingly delivers the best agreement with the data down to $\simeq 0.2$ MeV. Further applications of the underlying scheme were reported recently [10]. We note, however,

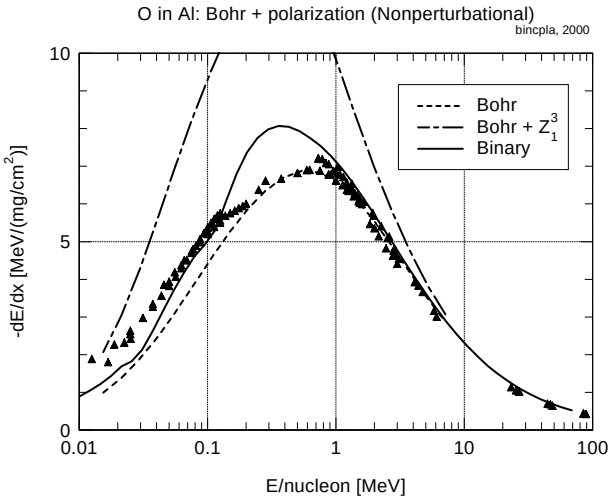

Fig. 10. Comparison of calculated equilibrium stopping forces with experimental data on O in Al compiled by Paul. Marked points refer to data from 16 different sources [21,26]. See text.

Table 1. Data utilized in characterizing target properties of Al. Columns 2 and 3 compiled by Mikkelsen from reference [24], leading to a whole-atom I-value of 164.14 eV. Column 4 from reference [25].

Shell	no. electrons	$\hbar\omega$(eV)	U(eV)
K	1.753	2795.47	1559.6
L	8.304	201.96	84.1
M	2.943	16.89	6.9

that this curve, as do the other two, ignores the shell correction as well as projectile excitation/ionization. Shell corrections have not yet been incorporated but are known to significantly lower the stopping force around the maximum. Conversely, projectile excitation/ionization gives rise to enhanced stopping when the number of electrons on the projectile becomes comparable with that on the target. The curve labelled "Bohr + Z_1^3" overestimates the stopping force by an amount that is unlikely to be compensated by the shell correction. The curve labelled "binary" improves the agreement down to lower velocities, and the slight overestimate around the maximum is of the order of the shell correction.

Also the transition to the Bethe regime needs attention. A pertinent correction [8] can be based on the Bloch theory [5,4]. The necessity of such a correction is clear from inspection of Figure 10 at energies/nucleon above 20 MeV.

This work has been supported by the Danish Natural Science Research Council (SNF). Discussions with Henning H. Mikkelsen at various stages of this work are gratefully acknowledged.

Appendix A: Electron trajectory in binary scattering

For scattering by a central-force potential, the radial part of the relative motion is determined by the relation

$$v\mathrm{d}t = \pm\frac{\mathrm{d}r}{\sqrt{1-2V(r)/mv^2-p^2/r^2}} \tag{25}$$

which follows from energy and angular-momentum conservation. Let the scattering plane be the $x-y$ plane. Then, for an incoming trajectory

$$x = vt; \quad y = p, \tag{26}$$

integration of equation (25) yields

$$r(t) = vt + 2\sqrt{r_m^2-p^2} - 2\int_{r_m}^{\infty}\mathrm{d}r \times\left(\frac{1}{\sqrt{1-2V(r)/mv^2-p^2/r^2}}-\frac{1}{\sqrt{1-p^2/r^2}}\right) \tag{27}$$

for the outgoing trajectory at distances where $V(r)$ is negligibly small.

Writing equation (27) in the form

$$r(t) = vt + 2\tau(p,v), \tag{28}$$

$\tau(p,v)$ being defined by equation (11), we find the asymptotic trajectory in relative coordinates,

$$x(t) = \Big[vt+2\tau(p,v)\Big]\cos\theta(p,v), \tag{29}$$

$$y(t) = \Big[vt+2\tau(p,v)\Big]\sin\theta(p,v), \tag{30}$$

and hence

$$x_\mathrm{e}(t) = vt - [vt+2\tau(p,v)]\cos\theta(p,v) \tag{31}$$

$$y_\mathrm{e}(t) = p - [vt+2\tau(p,v)]\sin\theta(p,v) \tag{32}$$

for the electron motion in the laboratory system.

The minimum value of $[x_\mathrm{e}(t)]^2+[y_\mathrm{e}(t)]^2$ delivers the distance $r_\mathrm{eff}(p,v)$ of the asymptotic trajectory from the origin as defined in Figure 3,

$$r_\mathrm{eff}^2 = \left(2\tau(p,v)\cos\frac{\theta(p,v)}{2} - p\sin\frac{\theta(p,v)}{2}\right)^2, \tag{33}$$

from where equation (12) follows, the sign being determined from the behavior at small scattering angles.

Appendix B: Perturbation expansion of the time integral

A procedure for perturbation expansion of classical scattering integrals has been developed in reference [22]. Writing the time integral equation (11) in the form

$$\tau(p,v) = \int_p^\infty \frac{\mathrm{d}r}{\sqrt{1-p^2/r^2}} - \int_{r_m}^\infty \frac{\mathrm{d}r}{\sqrt{1-2V(r)/mv^2-p^2/r^2}}, \tag{34}$$

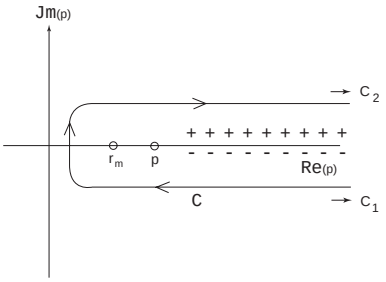

Fig. 11. Integration path $\mathcal{C}$ for time integral. Attractive interaction assumed.

we pull the path of integration into the complex plane in accordance with Figure 11. A cut is introduced along the positive x-axis from the lower limit of integration to infinity, the sign at the edges being defined in the figure. This leads to

$$\tau(p,v) = \frac{1}{2}\int_\mathcal{C}\mathrm{d}r\left(\frac{1}{\sqrt{1-p^2/r^2}} - \frac{1}{\sqrt{1-2V(r)/mv^2-p^2/r^2}}\right), \tag{35}$$

here a common integration path $\mathcal{C}$ has been chosen by making use of Cauchy's theorem.

Taylor expansion up to the first order in $V(r)$ then yields

$$\tau(p,v) = -\frac{1}{2mv^2}\int_\mathcal{C}\mathrm{d}r\frac{V(r)}{(1-p^2/r^2)^{3/2}} \tag{36}$$

or, after partial integration,

$$\tau(p,v) = -\frac{1}{2mv^2}\left[-\frac{1}{\sqrt{r^2-p^2}}r^2V(r)\Big|_{C_1}^{C_2} + \int_\mathcal{C}\frac{1}{\sqrt{r^2-p^2}}\frac{\mathrm{d}}{\mathrm{d}r}\left(r^2V(r)\right)\right]. \tag{37}$$

The first term in the brackets vanishes since *both* end points C_1 and C_2 of $\mathcal{C}$ lie at infinity. The remaining integral has an integrable singularity at $r=p$. Hence, the integration path can be pulled back to the real axis, and after insertion of equation (4) we obtain

$$\tau(p,v) = \frac{Z_1e^2}{mv^2}\int_p^\infty\frac{\mathrm{d}r}{\sqrt{r^2-p^2}}\left(1-\frac{r}{a_\mathrm{ad}}\right)\mathrm{e}^{-r/a_\mathrm{ad}} = \frac{Z_1e^2}{mv^2}\left[K_0\left(\frac{p}{a_\mathrm{ad}}\right)-\frac{p}{a_\mathrm{ad}}K_1\left(\frac{p}{a_\mathrm{ad}}\right)\right], \tag{38}$$

in agreement with equation (14).

Appendix C: Effective potential for dressed ion

The model potential (22) in conjunction with equation (23) was introduced in reference [11] on qualitative grounds: according to Bohr [6], equation (23) defines

the screening radius for a combination of two exponentially screened potentials. The present appendix serves to demonstrate that binary-scattering theory applied to this model potential rigorously reproduces the energy transfer predicted from Bohr theory for the potential (20). We may restrict our attention to the screening region ($r > a_\mathrm{s}$) in that context. Only the case of $a_\mathrm{s} < a_\mathrm{ad}$ is of practical interest since screening is ineffective for $a_\mathrm{s} > a_\mathrm{ad}$.

Bohr stopping theory in the perturbation limit for a screened-Coulomb potential of the form of equation (20) leads to [9]

$$T(p,v) = \frac{2Z_1^2 e^4 \omega^2}{mv^4}\left\{\left[\beta K_1(\zeta) + (1-\beta)\alpha K_1(\alpha\zeta)\right]^2 + \left[\beta K_0(\zeta) + \delta K_0(\alpha\zeta)\right]^2\right\} \quad (39)$$

with

$$\beta = \frac{q_1}{Z_1}, \qquad \zeta = \frac{\omega p}{v}, \qquad \alpha = \sqrt{1+\left(\frac{a_\mathrm{ad}}{a}\right)^2}. \quad (40)$$

Conversely, in the binary model the scattering angle for the potential equation (22) follows by generalization of equation (5)

$$\theta(p,v) = -\frac{2q_1e^2}{a_\mathrm{ad}mv^2}K_1\left(\frac{p}{a_\mathrm{ad}}\right) - \frac{2(Z_1-q_1)e^2}{amv^2}K_1\left(\frac{p}{a}\right) \quad (41)$$

in the small-angle approximation. The time integral may be found by generalization of equation (14),

$$\tau(p,v) = \frac{q_1e^2}{mv^2}\left[K_0\left(\frac{p}{a_\mathrm{ad}}\right) - \frac{p}{a_\mathrm{ad}}K_1\left(\frac{p}{a_\mathrm{ad}}\right)\right] + \frac{(Z_1-q_1)e^2}{mv^2}\left[K_0\left(\frac{p}{a}\right) - \frac{p}{a}K_1\left(\frac{p}{a}\right)\right], \quad (42)$$

and hence,

$$r_0(p,v) = 2\tau(p,v) - p\theta(p,v) = \frac{2q_1e^2}{mv^2}K_0\left(\frac{p}{a_\mathrm{ad}}\right) + \frac{2(Z_1-q_1)e^2}{mv^2}K_0\left(\frac{p}{a}\right). \quad (43)$$

Insertion of equations (41, 43) into

$$T(p,v) = \frac{1}{2}mv^2[\theta(p,v)]^2 + \frac{1}{2}m\omega^2[r_0(p,v)]^2 \quad (44)$$

is readily seen to reproduce equation (39).

Appendix D: Higher-order perturbation theory

Higher-order perturbations in classical binary-scattering theory were analysed by Lehmann and Leibfried [22]. The qualitative conclusion emerging from that work is that higher-order terms provide a good indicator of the limits of first-order perturbation theory but do not substantially extend its range of applicability in terms of impact parameter and/or velocity. We therefore restrict our attention to the leading (Z_1^3) correction, even though evaluation of terms of significantly higher than third order would be straight-forward. Expanding

$$\theta(p,v) = \theta_1(p,v) + \theta_2(p,v)... \quad (45)$$

$$\tau(p,v) = \tau_1(p,v) + \tau_2(p,v)... \quad (46)$$

in powers of the potential $V_\mathrm{eff}(r)$, equation (4) or equation (22), we find

$$T(p,v) = 2mv^2\sin^2\frac{\theta(p,v)}{2} = \frac{1}{2}mv^2\left[\theta_1(p,v)^2 + 2\theta_1(p,v)\theta_2(p,v)...\right] \quad (47)$$

and

$$W(p,v) = \frac{1}{2}m\omega^2 r_\mathrm{eff}(p,v)^2 = \frac{1}{2}m\omega^2\left\{\left[2\tau_1(p,v) - p\theta_1(p,v)\right]^2 + 2\left[2\tau_1(p,v) - p\theta_1(p,v)\right]\left[2\tau_2(p,v) - p\theta_2(p,v)\right]...\right\}. \quad (48)$$

$\theta_1(p,v)$ and $\tau_1(p,v)$ have been found in Section 2 and Appendix C. An expression for $\theta_2(p,v)$ may be found in reference [22],

$$\theta_2(p,v) = -\frac{1}{(mv^2)^2}\int_p^\infty \frac{r\,\mathrm{d}r}{p\sqrt{r^2-p^2}}\frac{\mathrm{d}^2}{\mathrm{d}r^2}\left(r^2V_\mathrm{eff}(r)^2\right), \quad (49)$$

and $\tau_2(p,v)$ has been determined by carrying out the calculation reported in Appendix B to the next order, resulting in

$$\tau_2(p,v) = -\frac{1}{2(mv^2)^2}\int_p^\infty \frac{\mathrm{d}r}{\sqrt{r^2-p^2}} \times \left(3\frac{\mathrm{d}}{\mathrm{d}r} + r\frac{\mathrm{d}^2}{\mathrm{d}r^2}\right)\left(r^2V_\mathrm{eff}(r)^2\right). \quad (50)$$

The screened potential equation (22) leads to

$$\theta_2(p,v) = -\frac{2}{\xi^2}\left[2\beta_1^2K_1(2\zeta) + 2(1-\beta_1)^2\alpha^2K_1(2\alpha\zeta) + (1+\alpha)^2\beta_1(1-\beta_1)K_1((1+\alpha)\zeta)\right] \quad (51)$$

and

$$2\tau_2(p,v) - p\theta_2(p,v) = \frac{6v}{\omega\xi^2}\left[\beta_1^2K_0(2\zeta) + (1-\beta_1)^2\alpha K_0(2\alpha\zeta) + (1+\alpha)\beta_1(1-\beta_1)K_0((1+\alpha)\zeta)\right]. \quad (52)$$

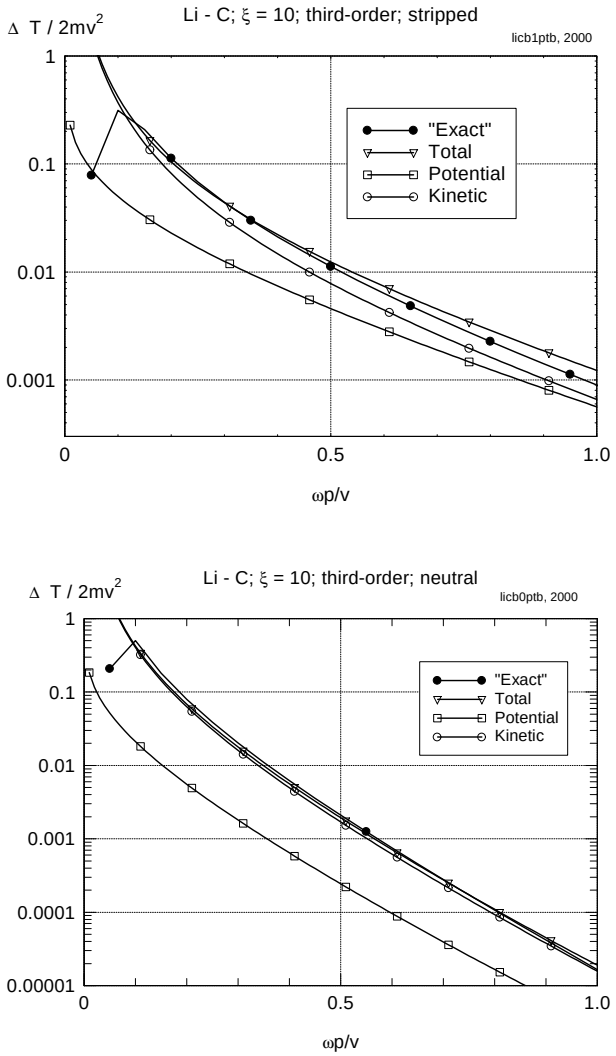

Fig. 12. Comparison of different approximations to Z_1^3 correction. "Exact": from reference [11]; kinetic: from equation (47); potential: from equation (48); total: sum of kinetic and potential; upper graph: stripped ion; lower graph: neutral projectile.

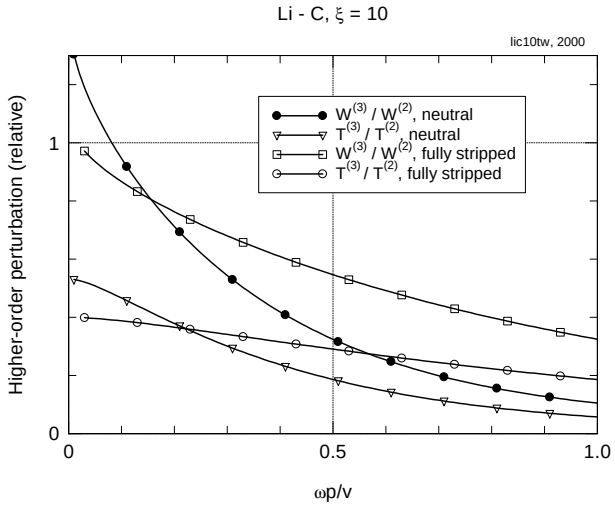

Fig. 13. Ratio of third-order to second-order contributions to energy loss in the binary model evaluated from equations (47, 48).

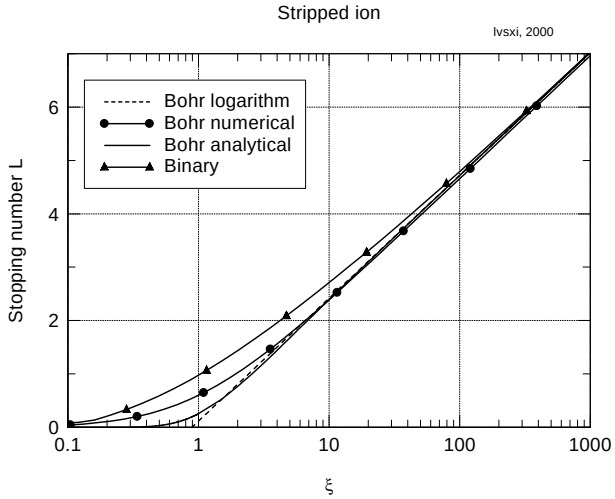

Fig. 14. Stopping number L for stripped ion *versus* Bohr parameter $\xi = mv^3/Z_1e^2\omega$ for four versions of the Bohr model. See text.

Figure 12 shows results for the system discussed in Figures 5 and 8. Comparison of the upper graph with Figure 5 shows near-perfect agreement between the binary evaluation and its perturbation expansion at large impact parameters, as it should be, and that agreement holds down to $\omega p/v \simeq 0.1$. The lower graph shows even better agreement for a neutral projectile, as was found already in Figure 8. Figure 13 shows the relative significance of the third-order perturbation in both the kinetic and the potential contribution. It is seen that both ratios drop off much more rapidly in case of the neutral projectile than for the stripped ion. Clearly, with a decreasing interaction force the significance of higher-order perturbations must decrease.

Appendix E: Approximate stopping numbers L(ξ) for point charge interacting with a harmonic oscillator

We conclude by adding another iteration to an ongoing series of approximations to the stopping number $L = L(\xi)$ in the Bohr model. Within the physical model (point charge interacting with one harmonically-bound target electron) $L(\xi)$ is a universal function [15]. In addition to Bohr's original logarithmic expression, Figure 14 shows the numerical interpolation given in reference [8] and an analytical formula mentioned in reference [23]. The rather large difference between the second and the third curve was noticed previously, and it was asserted that the true result was intermediate [9]. While this is presumably true within the lowest order of perturbation theory, higher-order perturbations raise the predicted curve significantly even above

the numerical interpolation, as is seen from the binary curve. We have not added a Z_1^3-corrected curve of the type discussed in reference [11] and included in Figure 7. While the dependence on impact parameter determined in that model has been very useful as a standard for comparison with the present approach, the accuracy of the predicted stopping numbers was estimated to $\sim 25\%$ in reference [11]. Figure 9 shows that those results lie systematically above the binary predictions, the difference reaching from a few per cent to $\sim 30\%$ over the range of ξ-values covered in the graph.

References

1. H. Bethe, Ann. Physik **5**, 324 (1930).
2. U. Fano, Ann. Rev. Nucl. Sci. **13**, 1 (1963).
3. P. Sigmund, Nucl. Instrum. Meth. B **135**, 1 (1998).
4. J. Lindhard, A.H. Sørensen, Phys. Rev. A **53**, 2443 (1996).
5. F. Bloch, Ann. Physik **16**, 285 (1933).
6. N. Bohr, Mat. Fys. Medd. Dan. Vid. Selsk. **18**, 1 (1948).
7. N. Bohr, Philos. Mag. **25**, 10 (1913).
8. P. Sigmund, Phys. Rev. A **54**, 3113 (1996).
9. P. Sigmund, Phys. Rev. A **56**, 3781 (1997).
10. H. Paul, A. Schinner, P. Sigmund, Nucl. Instrum. Meth. B **164-165**, 212 (2000).
11. A. Schinner, P. Sigmund, Nucl. Instrum. Meth. B **164-165**, 220 (2000).
12. P. Sigmund, Eur. Phys. J. D **12**, 111 (2000).
13. J.C. Ashley, R.H. Ritchie, W. Brandt, Phys. Rev. B **5**, 2393 (1992).
14. J.D. Jackson, R.L. McCarthy, Phys. Rev. B **6**, 4131 (1972).
15. J. Lindhard, Nucl. Instrum. Meth. **132**, 1 (1976).
16. A.F. Lifschitz, N. Arista, Phys. Rev. A **57**, 200 (1998).
17. J.A. Brinkman, J. Appl. Phys. **25**, 961 (1954).
18. G. Leibfried, *Bestrahlungseffekte in Festkörpern* (Teubner, Stuttgart, 1965).
19. M.T. Robinson, *Table of Classical Scattering Integrals*, Tech. Rep. ORNL-4556, Oak Ridge National Laboratory (1970).
20. W. Brandt, M. Kitagawa, Phys. Rev. B **25**, 5631 (1982).
21. M.J. Berger, H. Paul, in *Atomic and Molecular Data for Radiotherapy and Radiation Research* (International Atomic Energy Agency, Vienna, 1995), No. IAEA-TECDOC-799, Chap. 7, pp. 415–546.
22. C. Lehmann, G. Leibfried, Z. Phys. **172**, 465 (1963).
23. J.D. Jackson, *Classical Electrodynamics* (John Wiley & Sons, New York, 1975).
24. D.Y. Smith, E. Shiles, M. Inokuti, edited by E.D. Palik, *Handbook of Optical Constants of Solids* (Academic Press, Orlando, 1985), Vol. 1, p. 369.
25. K.D. Sevier, *Low Energy Electron Spectrometry* (Wiley, New York, 1972).
26. H. Paul, personal communication, 2000.